Phase-field simulations

by

Murtazo Nazarov

June 2006
Master of Science Thesis from
Royal Institute of Technology
Department of Mechanics
SE-100 44 Stockholm, Sweden

To my dear sister, Ohista

Acknowledgements

Taking this opportunity, first of all, I would like to say thanks to my supervisor Professor Gustav Amberg for his guidance, helps and encouragement. Thank you for giving me an opportunity to work in this interesting area and for joining me to your research group during my thesis work.

My special thanks to my second supervisor Minh Do-Quang for his suggestions, discussions, helps in understanding the subject and problems. Without his helps this thesis would be impossible to finish. Thank you, Minh!

Also, my great thanks to my family, my father and mother, for your love and support, your love makes me alive. Especially, to my brother Mustafo, your encouragements and support helped me to grow up from a pupil of a small village to a student and a part of research team in one of the largest scientific centers in the world.

I thank all my teachers in NADA, I gained a lot of knowledge on numerics and programming from you. I wish to thanks my best friends and group-workers Jelena, Sami and Nargis for sharing knowledge and friendship. I think we were one of the best groups in NADA.

My studies at KTH is financially supported by Swedish Institute (SI), which is gratefully acknowledged here.

Stockholm, June 2006

Murtazo Nazarov

Abstract

The modeling and simulation of the dendritic growth during solidification process of a pure material in two and three dimensional spaces are of a great interest in this thesis, as well as the fluid effect to the dendrite on the growth in two dimensional space.

For this reason the phase field model is used. To avoid some difficulties in the model, the semisharp phase field model is introduced. The inclusion of anisotropic surface energy is studied in both lands dimensions.

Furthermore, a convection effect of the fluid flow to the dendrite growth was studied. The Navier-Stokes equations are applied to solve velocity and pressure.

The obtained partial differential equations are solved numerically using an adaptive finite element method for unstructured triangular domain. The symbolic computational tool, FemLego is used for the calculations as it is easy to input the approximation form of the equations into a Maple input file. It is also easy to make an adaptive error control in finite elements of the problem in FemLego. In order to understand the shape of the resulting dendrites some figures are showed and discussed.

Keywords: Phase field model, semisharp, dendritic growth, adaptive finite element method, Navier-Stokes.

Contents

Chapter 1

Introduction

An example of evolution microstructure can be solidification, welding, melting, etc. This is a challenging area of research and also a subject of many articles published during the last decade. Studying and understanding the way in which dendrites grow will make the material engineers able to reach the desired properties of the manufactured materials in the future.

Many models have been developed to investigate the problem. Those models have good realistic results and can be applied to other phase transitions. In models of solidification, the interface of liquid/solid represents considerable difficulties for a numerical scheme. The position of interface has a complicated geometry. This position must be determined as a part of the solution procedure. The procedure makes the governing nonlinear problem formulations more difficult. The interface gives discontinuity to variables in the equations described by jump condition. Therefore, it is difficult to implement numerical schemes that are based on tracking the interface location explicitly.

Introducing an additional phase field variable is an alternative formulation for solidification problems. Many problems described above can be avoided in this case. The phase field variable is a smooth approximation to a characteristic function that assumes distinct constant value in each phase. The assumption is that $\phi = -1$ in liquid part and $\phi = 1$ in solid part. The tight transition regions are identified with the solid-liquid interface. Within these regions the phase field variable changes smoothly from -1 to 1. The interface is a diffuse, while it is considered sharp in other models. Therefore, other variables also change smoothly rather than discontinuously. The location of the interface is associated with the level lines of the phase field variable. However, the interface tracking is not required.

The governing equation is modified to include an additional evolution equation for the phase field. Assume the interface thickness tends to zero. Then the appropriate jump conditions across the sharp-interface limit are recovered.

Another phase field method, the semisharp phase field method is used in this thesis. The method is proposed by Gustav Amberg, [6]. The governing equations in the method are based on standard phase field model. Moreover, some modifications are done on this type of model. The interface to be identified with a phase field contour where changes in sharp and energy take place. Thus, the interface is "sharp" in some sense.

This master thesis applies the phase field model from the works of Gustav Amberg [6], and Robert Tönhardt [7]. The thesis consists of four chapters. The phase field and semisharp methods, some property of the models, numerical simulation for two and three dimensions, stability of numerical scheme for 2D and the computation results are discussed.

Chapter 2 gives a brief overview about mathematical model and numerical methods. The difficulties during numerical computations as well as the ways of solving them are outlined. First, the dendritic growth of crystal is studied. Moreover, the numerical difficulties, stability analysis, modification in semisharp, extending 2D problem to three dimensions for anisotropy formulation and some

numerical applications are studied. A consistent part of the chapter is the fluid flow in the melt part of dendrite and effects of the flow during its growth.

Other chapters include the obtained results in different cases and parameters, figures from simulations both in 2D and 3D cases with and without fluid flow as well as conclusions and discussion.

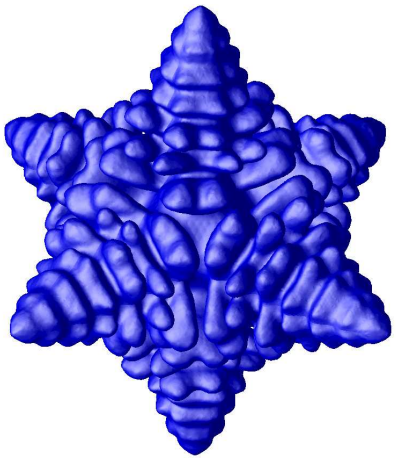

Figure 1.1: Three dimensional dendrite

Chapter 2

Mathematical model and numerical method

2.1 The Phase field model

A Stefan problem is a classical way of describing the solidification problem mathematically. In this problem the diffusion equations describe the transport of heat between the phases, solid and liquid, and boundary conditions specified in moving interface. Finding the analytical solution for the Stefan problem is difficult, since the shape of phases changes in time. Therefore, the numerical algorithm is developing since the last decades. [1]

The crystal shape using *front tracking technique* is considered. The idea is marking a finite set of points in interface. These points can be connected by interpolating polynomials to obtain the interface. Then the time-dependent heat equation in solid/liquid parts can be solved. The points in interface should be connected, deleted or refined, because of complicated shape of interface. This approach will be significantly more difficult if the spatial dimension increases.

Another approach is phase field, in which a sharp interface is replaced by continuous variations, which are measured by the phase field variables. The interface is determined by the value of phase field variables, the interface location does not need to be tracked explicitly. Consequently, the phase-field models are easier to implement computationally than the sharp-interface models, especially when complex interface morphologies are present. [2]

The phase field variable is defined as follows:

$$\phi(x,t) = \begin{cases} -1, & x \in \Omega_-(t), \\ 1, & x \in \Omega_+(t). \end{cases}$$

where -1 denotes liquid phase and 1 solid phase. The sharp interface of width zero is replaced by a diffuse interface with width W in which the phase variable smoothly changes value from -1 to 1, Figure 2.1. The interface is defined as the level set of points satisfying $\phi(\bar{x},t) = C_i$, where $-1 < C_i < 1$.

The non-dimensional phase field method developed by Wheeler [3] is used in this thesis. This method is thermodynamically consistent and captures the sharp interface model with width of the interface goes to zero. The following equation is a modified heat equation in Stefan problem:

$$\frac{\partial \theta}{\partial t} + \frac{30 g(\phi)}{\Delta_c} \frac{\partial \phi}{\partial t} = \nabla^2 \theta, \tag{2.1}$$

where ϕ corresponds to the latent heat and $g(\phi) = \phi^2(1-\phi)^2$. The Stefan-condition is used

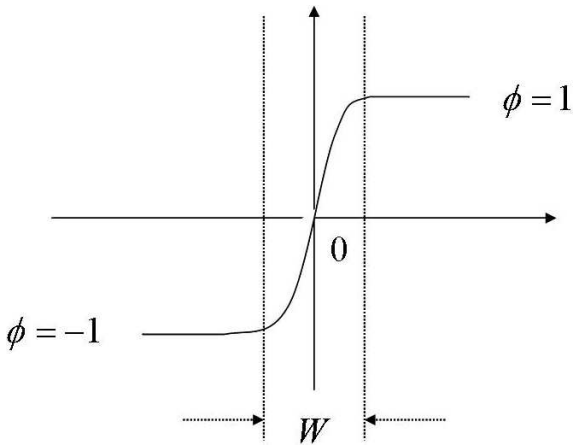

Figure 2.1: Schematic of an interface of phase field in 1D. The liquid phase has a value of $\phi = -1$, a smooth transition through the interface and a value of the solid $\phi = 1$.

as a boundary condition, in which the velocity of the solid/liquid interface is defined as $V_n = \Delta_c \left(\frac{\partial\theta}{\partial n}\right)_{liquid}^{solid}$. Here n is the normal of the interface into liquid, V_n is dimensionless normal velocity of the interface into liquid and $\Delta_c = c\Delta T/L$ is dimensionless undercooling, or Stefan number. We have an extra transport equation, which is a modified Gibbs-Thomson condition:

$$\frac{\epsilon^2}{m}\frac{\partial\phi}{\partial t} = \epsilon^2\nabla_a^2\phi + 30A\Delta_c\epsilon\theta g - \frac{1}{4}\dot{g} \tag{2.2}$$

The following parameters are used in the equations above:

$\epsilon = \delta/W$ - the dimensionless width of the interface;

$\nabla_a^2\phi$ - the Laplacian;

$A = \frac{\sqrt{2}W}{12d_0}$ - the width of interface divided by capillary length;

$m = \frac{\mu d_0 T_m}{\alpha}$ - a parameter, which depends on the kinetic coefficient, μ;

2.1.1 Anisotropy term

In isotropic formulation the surface energy is independent of local interface orientation. Then the term, ∇_a^2, in equation (2.2) is a simple Laplacian. However, for many materials the surface energy depends on the local interface orientation. Metals are example of this kind of materials. In this case we represent an anisotropic surface energy by the following formula:

$$\sigma = \sigma_0\eta(\overrightarrow{n}), \tag{2.3}$$

here the term $\eta(\overrightarrow{n})$ describes the dependence of the surface energy on the local interface orientation trough the vector $\overrightarrow{n}$. [4].

In two dimensional space the surface energy can be found as follows:

$$\eta(\overrightarrow{n}) = 1 + \gamma\cos(4\beta), \tag{2.4}$$

where $\beta = \arctan\left(\frac{\partial\phi}{\partial y}/\frac{\partial\phi}{\partial x}\right)$ an angle between the interface and orientation of the contours, γ is the strength of anisotropy.

The 2D Laplacian, $\nabla_a^2\phi$, in equation (2.2) has been modified as:

$$\nabla_a^2\phi = \nabla\cdot\left(\eta^2\nabla\phi\right) - \frac{\partial}{\partial x}\left(\eta\dot{\eta}\frac{\partial\phi}{\partial y}\right) + \frac{\partial}{\partial y}\left(\eta\dot{\eta}\frac{\partial\phi}{\partial x}\right), \tag{2.5}$$

where $\dot{\eta} = \frac{d\eta}{d\beta}$ - differentiation with respect to β. Then, for anisotropic case the equation (2.2) can be written as follows:

$$\frac{\epsilon^2}{m}\frac{\partial\phi}{\partial t} = \epsilon^2\nabla\cdot\left(\eta^2\nabla\phi\right) - \epsilon^2\frac{\partial}{\partial x}\left(\eta\dot{\eta}\frac{\partial\phi}{\partial y}\right) + \epsilon^2\frac{\partial}{\partial y}\left(\eta\dot{\eta}\frac{\partial\phi}{\partial x}\right) + 30A\Delta_c\epsilon\theta g - \frac{1}{4}\dot{g}. \tag{2.6}$$

The three dimensional phase field model is simulated in this thesis work, as well. We are interested to study both isotropic and anisotropic cases. In isotropic case the phase field equations in 3D have the same definition as equations (2.1) and (2.2). The anisotropy term in 3D can be expressed as the following formula [5]:

$$\eta(\phi_x,\phi_y,\phi_z) = (1-3\gamma)\left(1 + \frac{4\gamma}{1-3\gamma}\frac{\phi_x^4+\phi_y^4+\phi_z^4}{|\nabla\phi|^4}\right). \tag{2.7}$$

Then the Laplacian in three dimensions should be replaced with the following anisotropy Laplacian

$$\nabla_a^2\phi = \frac{\partial}{\partial\phi_x}\left(|\nabla\phi|^2\eta\frac{\partial\eta}{\partial\phi_x}\right) + \frac{\partial}{\partial\phi_y}\left(|\nabla\phi|^2\eta\frac{\partial\eta}{\partial\phi_y}\right) + \frac{\partial}{\partial\phi_z}\left(|\nabla\phi|^2\eta\frac{\partial\eta}{\partial\phi_z}\right) + \nabla\cdot\left(\eta^2\nabla\phi\right) \tag{2.8}$$

2.1.2 Semisharp Phase field method

In the standard sharp interface method the interface between two phases is represented by a surface with no internal structures or width. The standard phase field model requires an asymptotic analysis for vanishing interface. In order to have the result proper to interface kinetics, the interface width should be smaller then the capillary length, which is in order of nanometers. Therefore, modification of the model should be done for developing and extending this analysis.

The semisharp phase field method was proposed by Amberg [6], in which some modifications are made in model equations. The purpose of modifications is to solve the modified equation analytically.

To clarify the idea, the following single isotropic model is studied. For simplicity, the thermal solidification of pure material is assumed. The Gibbs-Thomson kinetics at the interface is defined as $-\theta_i = V/\mu + d_0/R$, where V is the normal speed of interface, d_0 is the capillary length. The nondenominational temperature is assumed according to $\theta = c(T-T_m)/L$, length with an arbitrary reference length H, time with H^2/κ. Here, c is a specific heat, T_m is a temperature of a flat interface, L is a latent heat, and κ is a heat diffusivity.

Then, the phase field model is written as following equations:

$$\tau\frac{\partial\phi}{\partial t} = W^2\nabla^2\phi - f'(\phi) - g'_\delta(\phi)h(\lambda\theta), \tag{2.9}$$

$$\frac{\partial\theta}{\partial t} = \nabla^2\theta + \frac{\partial g_\delta(\phi)}{\partial t}. \tag{2.10}$$

Here the ϕ is a phase variable defined as above, W is the interface width, τ is linked to kinetic undercooling. In the standard method, (2.2), the functions $f(\phi)$ and $g_\delta(\phi)$ are defined as follows:

$$f(\phi) = (1-\phi)^2(1+\phi)^2,$$

$$g_\delta(\phi) = \frac{15}{16}\left(\frac{\phi^5}{5} - 2\frac{\phi^3}{3} + \phi\right) + \frac{1}{2}.$$

As we can see the function $f(\phi)$ has minimum at the points $\phi = \pm 1$ and $g_\delta(\phi)$ increases from 0 to 1 when ϕ changes the value from -1 to 1. The function $h(\lambda\theta)$ is chosen as $h(\lambda\theta) = \lambda\theta$.

Then some important modifications were used for standard phase field model. The function $g_\delta(\phi)$ is chosen as a smoothed step function, which jumps from 0 to 1 over the interval with width δ, Figure 2.3. The semisharp model is obtained when $\delta = 0$. We choose the function $f(\phi)$ simpler, in order to evaluate the kinetics of the model exactly:

$$f(\phi) = \begin{cases} (\phi - 1)^2, & \text{for} \phi > 0, \\ (\phi + 1)^2, & \text{for} \phi < 0. \end{cases}$$

$$g_\delta(\phi) = \frac{\phi}{\sqrt{\phi^2 + \delta^2}};$$

Then an explicit choice of the function $h(\lambda\theta)$ is made using these functions. In [6], these functions are found analytically, which are $h(\lambda\theta) = \lambda\theta$

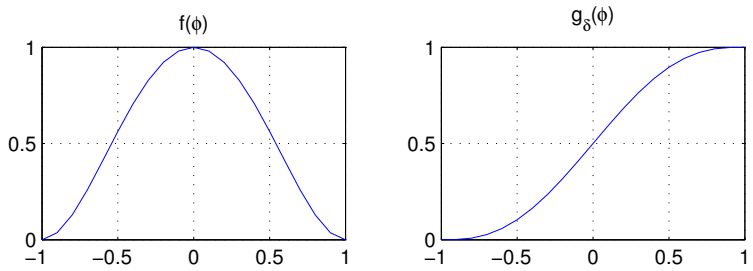

Figure 2.2: The choice of functions $f(\phi)$ and $g_\delta(\phi)$ in standard phase field method.

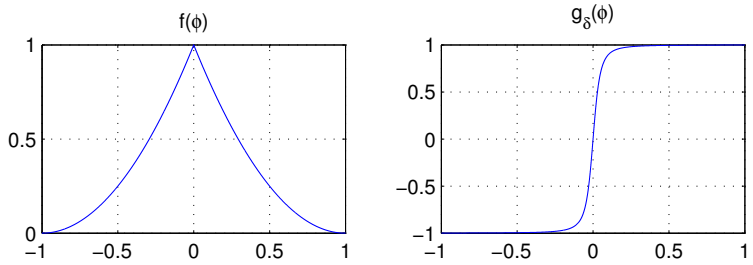

Figure 2.3: The choice of functions $f(\phi)$ and $g_\delta(\phi)$ in semisharp phase field method.

The interface is studied when $\phi = 0$, so interface is sharp in this sense. It has been showed that this model gives Gibbs-Thomson kinetics with the temperature precisely at interface, $\phi = 0$. This thesis also studies the isotropic equation (2.9), (2.10). The simulation is done for different parameters. Then the anisotropic case is studied.

2.2 Navier-Stokes equations

The Navier-Stokes equations are:

$$\frac{\partial u_i}{\partial t} + u_j \frac{\partial u_i}{\partial x_j} = -\frac{1}{\rho}\frac{\partial p}{\partial x_i} + \nu \frac{\partial^2 u_i}{\partial x_j \partial x_j}, \tag{2.11}$$

$$\frac{\partial u_i}{\partial x_i} = 0, \tag{2.12}$$

where, ρ is the density, ν is the kinematic viscosity. We are interested in non-dimensional form of Navier-Stokes equations, because it is convenient for our simulation. We use the following

non-dimensional variables and scales:

$$x_i^* = \frac{x_i}{L}, \quad t^* = \frac{t}{T_0}, \quad u_i^* = \frac{u_i}{U_0}, \quad p^* = \frac{p}{p_0}, \quad \frac{\partial}{\partial x_i} = \frac{1}{L}\frac{\partial}{\partial x_i^*}, \quad \frac{\partial}{\partial t} = \frac{1}{T_0}\frac{\partial}{\partial t_i^*},$$

where $*$ denotes the non-dimensional variable. We introduce the non-dimensional variables into Navier-Stokes equation (2.11) and obtain:

$$\frac{U_0}{T_0}\frac{\partial u_i^*}{\partial t^*} + \frac{U_0^2}{L}u_j^*\frac{\partial u_i^*}{\partial x_j^*} = -\frac{p_0}{\rho L}\frac{\partial p^*}{\partial x_i^*} + \nu\frac{U_0^2}{L^2}\frac{\partial^2 u_i^*}{\partial x_j^* \partial x_j^*}, \tag{2.13}$$

$$\frac{U_0}{L}\frac{\partial u_i^*}{\partial x_i^*} = 0. \tag{2.14}$$

We simplify these equations and drop the sign of non-dimensional variables, we find:

$$\frac{\partial u_i}{\partial t} + \frac{U_0 T_0}{L}u_j\frac{\partial u_i}{\partial x_j} = -\frac{1}{\rho}\frac{\partial p}{\partial x_i} + \nu\frac{T_0}{L^2}\frac{\partial^2 u_i}{\partial x_j \partial x_j}, \tag{2.15}$$

$$\frac{\partial u_i}{\partial x_i} = 0. \tag{2.16}$$

Now, we introduce some new parameters:

$$\alpha = \frac{L^2}{T_0}, \quad T_0 = \frac{L}{U_0}, \quad Pe = \frac{U_0 L}{\alpha}, \quad \mathrm{Pr} = \frac{\nu}{\alpha}, \quad \Rightarrow$$

$$\frac{U_0 T_0}{L} = \frac{U_0 L T_0}{L^2} = \frac{U_0 L}{\alpha} = Pe, \quad \frac{\nu T_0}{L_0} = \frac{\nu}{\alpha} = \mathrm{Pr},$$

here, α is the kinematic viscosity or the momentum diffusivity. Also, the pressure is scaled as $p = \frac{p}{p_0}\frac{L}{\rho U_0 \alpha} = \frac{T_0}{\rho U_0 L}$. Then, we obtain the non-dimensional Navier-Stokes equations:

$$\frac{\partial u_i}{\partial t} + Pe u_j\frac{\partial u_i}{\partial x_j} = -\frac{\partial p}{\partial x_i} + \mathrm{Pr}\frac{\partial^2 u_i}{\partial x_j \partial x_j}, \tag{2.17}$$

$$\frac{\partial u_i}{\partial x_i} = 0. \tag{2.18}$$

2.3 Flow around the dendrite

The convection due to the melt flow in solidification is unavoidable, and the effects of convection on the micro/macro-structures and various properties of the solidified metal and alloys can be significant. Melt flow in solidification can be categorized into natural (or free) and forced convection. The natural convection can be seen in a case when the densities of the solid and liquid are different regardless of the presence of the gravitational force. Forced convection is induced by electromagnetic stirring, rotation, pouring of the melt, an anti-parallel flow to the direction of motion of the tip, etc., some of which intentionally applied to cause convection to enhance solute transport from the solid-liquid interface in order to reduce macro and micro segregation. If the natural convection is strong enough, then the micro-structure is affected and the properties of the solidified material changes.

In practice and in experiments it is difficult to avoid convection. Convection in the melt modifies the diffusion fields, the kinetics of the interface and the amount of defects in the solid. Therefore, it is important to study various types of flows that are present during solidification.

The simulation of the convection during the solidification in this thesis is based on the works of Tönhardt and Amberg [9, 10]. Their results show that the evolution of the dendrite shape was altered by the flow, and the growth of the side branches was promoted on the upstream side and inhibited on the downstream side as expected.

We assume anti-parallel fluid flow to the direction of motion of the tip in dendrite. The only changes should be done in temperature equation, (2.10), and momentum equations, (2.17).

That is, the temperature equation with convective term can be changed as:

$$\frac{\partial \theta}{\partial t} + Pe\bar{u} \cdot \nabla\theta = \nabla^2\theta + \frac{\partial g_\delta(\phi)}{\partial t}, \tag{2.19}$$

where, $Pe = UW/\alpha$ is the Peclet number defined from above, $\overline{u}$ is a non-dimensional velocity in the domain, where dendrite grows. The convective term is present in the liquid phase only.

The dynamic viscosity, ν, is replaced with the following expression:

$$\nu = \nu_0(1 + f_\nu), \tag{2.20}$$

where, ν_0 is the tabulated viscosity of the melt, and the function f_ν depends on the phase field variable ϕ and its purpose is to increase viscosity for the solid part. In our simulations we use the following definition of function f_ν

$$f_\nu(\phi) = \begin{cases} 1 & \text{for} \quad \phi < 0, \\ 1 + (\phi + 1) \cdot 1000 & \text{for} \quad \phi \geq 0. \end{cases} \tag{2.21}$$

We assume the melt is incompressible. The governing Navier-Stokes equations for flow around the dendrite in the melt are written as:

$$\frac{\partial u_i}{\partial t} + Peu_j\frac{\partial u_i}{\partial x_j} = -\frac{\partial p}{\partial x_i} + \Pr\frac{\partial}{\partial x_j}\left(f_\nu\left[\frac{\partial u_i}{\partial x_j} + \left(\frac{\partial u_i}{\partial x_j}\right)^*\right]\right), \tag{2.22}$$

$$\frac{\partial u_i}{\partial x_i} = 0. \tag{2.23}$$

where, Pr is Prandt number and * means the transpose of the operator.

2.4 Numerical treatments

As mentioned above, all equations in this thesis are simulated using toolbox FemLego. This toolbox was written by Gustav Amberg and being developing during the several years in the Department of Mechanics, KTH. [7], [8]. The toolbox consists of two parts: Maple procedures; FORTRAN and C routines.

The model, initial and boundary conditions are entered into Maple. Then, Maple generates the FORTRAN and C routines according to adapting Finite Element Methods for unstructured grids. The toolbox can be used in 1, 2 and 3 dimensions problems.

2.4.1 Stability analysis for phase field model

All our simulations are done using the finite element method for unstructured grid. Prior to numerical simulation we are interested in the stability condition of the model (2.9) and (2.10). In this respect, the obtained stability condition for finite difference method is valid for the finite element method, also. The Von-Neumann stability analysis is used to find the restriction for time-dependent problem above. Usually, the expression in right hand side in (2.9) and (2.10) is very nonlinear. Therefore, the linearization of the equation is necessary.

The equations (2.9) and (2.10) with the given functions $f(\phi)$ and $g_\delta(\phi)$ can be written as:

$$\begin{aligned} \tau\frac{\partial \phi}{\partial t} &= W^2\nabla^2\phi + 4\phi(1-\phi)(1+\phi) - \frac{15}{16}(\phi^4 - 2\phi^2 + 1)\lambda\theta, \\ \frac{\partial \theta}{\partial t} &= \nabla^2\theta + \frac{15}{16}(\phi^4 - 2\phi^2 + 1)\frac{\partial \phi}{\partial t}. \end{aligned} \tag{2.24}$$

We introduce the small perturbations $\tilde{\phi}$, $\tilde{\theta}$ around points ϕ_0 and θ_0. The interesting task is to investigate the local stability analysis when $\phi_0 = 0$ and $\theta_0 = 0$. Since, the perturbation is too small the terms $\tilde{\phi} \cdot \tilde{\theta}$, $\tilde{\phi}^n$, $\tilde{\theta}^n$ will be vanish. Hence, we obtain the following system of equations:

$$\begin{aligned} \tau \frac{\partial \tilde{\phi}}{\partial t} &= W^2 \nabla^2 \tilde{\phi} - \frac{15}{16} \lambda \tilde{\theta}, \\ \frac{\partial \tilde{\theta}}{\partial t} &= \nabla^2 \tilde{\theta} + \frac{15}{16} \frac{\partial \tilde{\phi}}{\partial t}. \end{aligned} \tag{2.25}$$

We assume $\phi = \tilde{\phi}$, $\theta = \tilde{\theta}$ and using the central difference for space and forward difference approximation for time we obtain:

$$\begin{aligned} \tau \frac{\Phi_{ij}^{n+1} - \Phi_{ij}^n}{\Delta t} &= W^2 \frac{1}{\Delta x^2} \left(\Phi_{i+1,j}^n - 2\Phi_{i,j}^n + \Phi_{i-1,j}^n \right) + \\ &+ W^2 \frac{1}{\Delta y^2} \left(\Phi_{i,j+1}^n - 2\Phi_{i,j}^n + \Phi_{i,j-1}^n \right) - \frac{15}{16} \lambda \Theta_{i,j}^n, \\ \frac{\Theta_{ij}^{n+1} - \Theta_{ij}^n}{\Delta t} &= W^2 \frac{1}{\Delta x^2} \left(\Theta_{i+1,j}^n - 2\Theta_{i,j}^n + \Theta_{i-1,j}^n \right) + \\ &+ W^2 \frac{1}{\Delta y^2} \left(\Theta_{i,j+1}^n - 2\Theta_{i,j}^n + \Theta_{i,j-1}^n \right) + \frac{15}{16} \frac{1}{\Delta t} \left(\Phi_{i,j}^{n+1} - \Phi_{i,j}^n \right). \end{aligned} \tag{2.26}$$

Where, Δx and Δy are distance between the grid-points along x and y axis, respectively, and Φ_{ij}^n is the numerical approximation of the solution $\phi(x_i, y_j)$ at the time $t = t_n$.

Now, we make the following ansatz:

$$\begin{aligned} \Phi_{ij}^n &= A^n \hat{\phi} e^{Ik_x i \Delta x} \cdot e^{Ik_y j \Delta y}, \\ \Theta_{ij}^n &= A^n \hat{\theta} e^{Ik_x i \Delta x} \cdot e^{Ik_y j \Delta y}, \end{aligned} \tag{2.27}$$

Here, $I = \sqrt{-1}$ is the imaginary unit, $A = |A| e^{-I\omega \Delta t}$ where ω is frequency, k_x and k_y are the wave numbers. Assuming $\alpha = k_x \Delta x$, $\beta = k_y \Delta y$, insert the ansatz (2.27) into finite difference equations (2.26), divide the obtained equations to the similar term $A^n e^{Ik_x i \Delta x} \cdot e^{Ik_y j \Delta y}$, and obtain:

$$\begin{aligned} \frac{\tau}{\Delta t}(A-1)\hat{\phi} &= W^2 \frac{2}{\Delta x^2}(\cos\alpha - 1)\hat{\phi} - W^2 \frac{2}{\Delta y^2}(\cos\beta - 1)\hat{\phi} - \frac{15}{16}\lambda\hat{\theta}, \\ \frac{1}{\Delta t}(A-1)\hat{\theta} &= W^2 \frac{2}{\Delta x^2}(\cos\alpha - 1)\hat{\theta} - W^2 \frac{2}{\Delta y^2}(\cos\beta - 1)\hat{\theta} + \frac{15}{16}\frac{1}{\Delta t}(A-1)\hat{\phi}, \end{aligned} \tag{2.28}$$

Then, the last system of linear equation should be solved. We are interested in nontrivial case, i.e. we strive for finding a value for A, in which the determinant of (2.28) is zero. Therefore, we solved the obtained quadratic equation for variable A. The Von-Neumann stability analysis requires $|A| \leq 1$ for a stable solution. Finally, we found that the explicit scheme (2.26) is stable if

$$\Delta t \leq C \frac{1}{\frac{1}{\Delta x^2} + \frac{1}{\Delta y^2}}$$

Where C is a constant, which can be calculated from the parameters of the system.

The same discussion is used for implicit scheme in finite difference, and we found that in stability there is no any restriction for Δt. The implicit scheme is always stable.

2.4.2 Discontinuity integrals in 2D and 3D

The interface contour between solid/liquid in semisharp mode is defined when $\phi = 0$. In [6] it is shown, that the jump in function g_δ generates a jump in the gradient of ϕ, and can be represented

as a following expression:

$$\frac{W^2}{2}\left[\left(\frac{d\phi^+}{dz}\right)^2-\left(\frac{d\phi^-}{dz}\right)^2\right]=h(\lambda\theta_i), \tag{2.29}$$

where, θ_i is the value of the temperature at the interface, and the z axis is chosen with origin at the interface.

This jump can be implemented in finite elements by adding a line integral of $W\lambda\theta$ along the interface in two dimensional case. In 3D the line integral is replaced into integration over a surface along the interface, Figure 2.4. It can be done easily by adding some modification in code. The possible cases in 3D are integration over a triangle and quadrangular, Figure 2.5 and Figure 2.6.

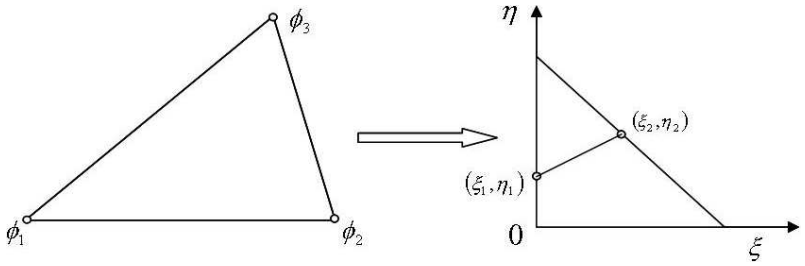

Figure 2.4: The points where $\phi = 0$ is found in the unit coordinate system, if $\phi_1 \cdot \phi_2 \cdot \phi_3 < 0$. The integration over the triangle $\Delta\phi_1\phi_2\phi_3$ is changed to integration over the line $(\xi_1,\eta_1),(\xi_2,\eta_2)$.

The idea is to find the triangular (tetrahedral) elements, which are on the interface. In these elements, there are some points, in which $\phi = 0$, i.e. the interface contour goes through the element. Then, corresponding coordinates for these points, $(\xi_1,\eta_1),(\xi_2,\eta_2)$, in unit coordinate system (ξ,η) should be found. After that, instead of calculating the integration over the element in finite elements, an integration over the line $(\xi_1,\eta_1),(\xi_2,\eta_2)$ is computed. The same discussion is done for 3D case.

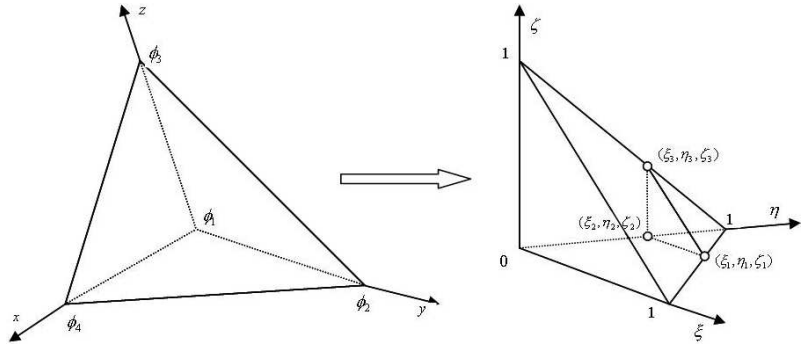

Figure 2.5: The points where $\phi = 0$ is found in the unit coordinate system, if $\phi_1 \cdot \phi_2 \cdot \phi_3 \cdot \phi_4 < 0$. In this case, the integration is done over the triangle with corners $(\xi_1,\eta_1,\zeta_1),(\xi_2,\eta_2,\zeta_2),(\xi_3,\eta_3,\zeta_3)$.

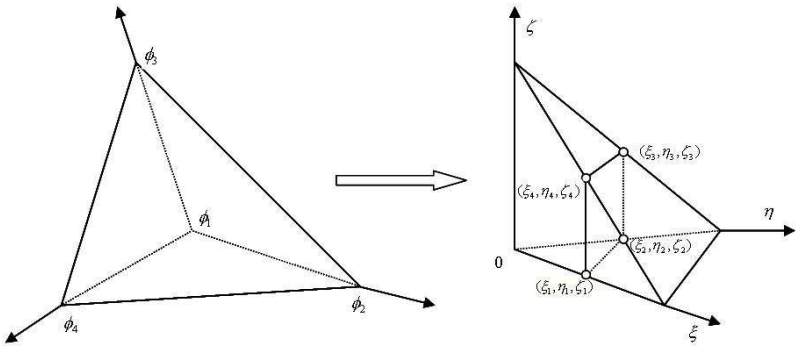

Figure 2.6: This figure describes the points, where $\phi = 0$ in the unit coordinate system, if two values of $\phi_i, i = 1, 2, 3, 4$ are positive and two others are negative. The integration is done over the quadrature with corners $(\xi_1, \eta_1, \zeta_1), (\xi_2, \eta_2, \zeta_2), (\xi_3, \eta_3, \zeta_3), (\xi_4, \eta_4, \zeta_4)$.

This modification is added using C functions to FemLego, and some changes are made in Maple procedure. The expression

$$ElementInt(DiscInt\,(\phi(x,y,z),(test(x,y,z)\cdot W\cdot\lambda\theta(x,y,z)))$$

is added to the phase field equation.

2.4.3 Numerical methods

The same technique of numerical method in [9] for solving equations (2.2), (2.19), (2.22), (2.23) is used in our simulations.

The above-mentioned equation is transformed to the discrete formulation using Galerkin formulation of finite element method. The basis functions are chosen linearly: triangles in 2D and tetrahedrons in 3D. The basis and test function are chosen from the same functional space.

The Navier-Stokes equations are solved using a fractional-step projection method proposed by J.L. Guermond and L. Quartapelle. It replaces the continuity equation into Poisson equation for pressure. The first step is viscous convection-diffusion step and the following FEM variational formulation is entered into the Maple input file:

$$\int_\Omega \frac{\bar{u}^* - \bar{u}_0}{\Delta t} v d\Omega + Pe \int_\Omega v\nabla\bar{u}^* d\Omega = \int_\Omega \nabla v(2P_0 - P_{00})d\Omega - \mathrm{Pr}\int_\Omega \nabla v\nabla\bar{u}^* f_\nu(\phi_0)d\Omega. \tag{2.30}$$

Then the pressure is updated using the following equation:

$$\int_\Omega \nabla(2P - P_0)\nabla v d\Omega = -\frac{1}{\Delta t}\int_\Omega v\nabla\bar{u}^* d\Omega - \int_\Omega \epsilon_p \nabla P\nabla v d\Omega. \tag{2.31}$$

The convection step is a last part of the fractional-step projection method, and determines the divergence free end-of-step velocities:

$$\int_\Omega \bar{u} v d\Omega = \int_\Omega \bar{u}^* v d\Omega - \Delta t\int_\Omega (\nabla(P - P_0)v + \epsilon_p\nabla P v)d\Omega. \tag{2.32}$$

In above formulation, v is the test function used in FEM variational formulation. As we can notice, the convection and diffusion terms are implicit and the time derivatives are descritized using the first order approximation. In each timestep, the descritized equations are solved using the GMRES (General Minimal Residual) or the ICCG (Incomplete Cholesky Conjugate Gradient) methods.

The variational form for the equation (2.2), (2.19) are written as the following equations:

$$\tau \int_\Omega \frac{v(\phi-\phi_0)}{\Delta t} d\Omega = -0.5W^2 \left[\int_\Omega v \nabla_a^2 \phi_0 d\Omega + \right.$$
$$+ \int_\Omega v \left[(\phi_0 - 1)(1 + sign(\phi_0)) + (\phi_0 + 1)(1 - sign(\phi_0)) \right] d\Omega \qquad (2.33)$$
$$\left. + \int_\Omega DiscInt(\phi_0, W\lambda\theta) d\Omega \right].$$

The function $sign(\phi_0)$ is used to define the sign of ϕ_0. The $\nabla_a^2\phi$ is anisotropy Laplacian from above, and it is a simple Laplasian for isotropic case. In anisotropic dendritic growth this term can be derived as the following formula in variation formulation, in 2D:

$$\int_\Omega v \nabla_a^2 \phi_0 d\Omega = \int_\Omega \eta\dot{\eta} \left(\frac{\partial \phi_0}{\partial y}\frac{\partial v}{\partial x} - \frac{\partial \phi_0}{\partial x}\frac{\partial v}{\partial y} \right) d\Omega + \int_\Omega \eta^2 \cdot \nabla v \cdot \nabla \phi_0 d\Omega, \qquad (2.34)$$

and for 3D case:

$$\int_\Omega v \nabla_a^2 \phi_0 d\Omega = \int_\Omega |\nabla \phi_0|^2 \eta \left(\frac{\partial \eta}{\partial \phi_x^0}\frac{\partial v}{\partial x} + \frac{\partial \eta}{\partial \phi_y^0}\frac{\partial v}{\partial y} + \frac{\partial \eta}{\partial \phi_z^0}\frac{\partial v}{\partial z} \right) d\Omega +$$
$$+ \int_\Omega \eta^2 \cdot \nabla v \cdot \nabla \phi_0 d\Omega. \qquad (2.35)$$

Here, $\phi_{x_i}^0 = \frac{\partial \phi_0}{\partial x_i}$, $x_i = x, y, z$.

The variational form for the temperature equation is derived as the follows:

$$\int_\Omega \frac{v(\theta-\theta_0)}{\Delta t} d\Omega = -\int_\Omega \kappa \nabla v \cdot \nabla \left(\theta + (1 - CN_\alpha)\theta_0 \right) d\Omega - Pe \int_\Omega v \bar{u}_c \cdot \nabla \theta d\Omega +$$
$$+ \int_\Omega v \frac{g(\phi) - g(\phi_0)}{\Delta t} d\Omega + \int_{\partial\Omega} v \cdot q_{BCval} dS, \qquad (2.36)$$

where $\bar{u}_c$ is the correction velocity from (2.32), CN_α the Courant number, κ - is the scaled interface curvature, q_{BCval} is read from the mesh and can give different values on different parts of the boundary and can be used in the boundary integrals in variational form.

As mentioned above, the width of interface is much smaller then other length scales. Therefore, using adaptive unstructured mesh in our calculation will be efficient. Initially, the computational domain is descretized with large triangular elements in 2D, and tetrahedrons in 3D, and then the interface region gets the highest resolution. As the interface evolves during the calculation, the mesh is adaptively changes by splitting or merging the elements according to an error function:

$$ErrCrit = \int_\Omega (Err_{Fact} |\nabla \phi|^2 + Err_{Fact_2} |\nabla \theta|^2) d\Omega, \qquad (2.37)$$

where, Err_{Fact} and Err_{Fact_2} are the parameters in order $\sim \frac{1}{W^2}$ and $\sim \frac{1}{100W^2}$, respectively. W is an interface width.

2.4.4 Computational domain

The computational domain in our simulation is the following figure:

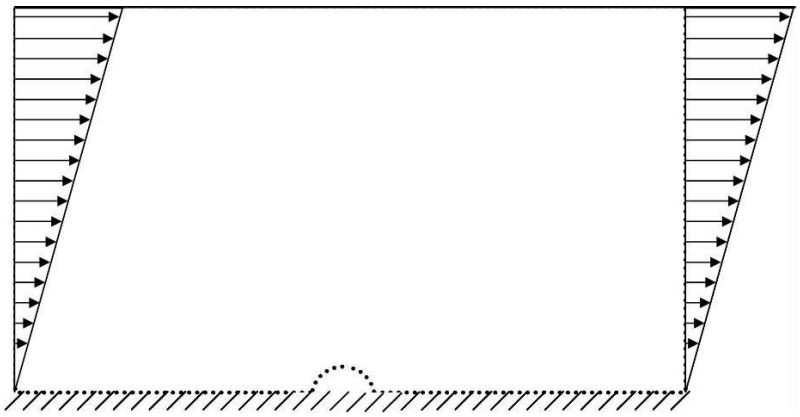

Figure 2.7: Computational domain

The initial value for dendrite is chosen as a small circle with radius $r = 0.03573$. The size of the domain is $-4 \leq x \leq 4$, $0 \leq y \leq 4$, but in some simulations the bigger domain size is used, also.

The following boundary condition is used in our computation:

1. For phase variable ϕ and temperature, the Neumann boundary condition is put for all boundaries:

$$\frac{\partial \phi}{\partial n} = 0, \qquad \frac{\partial \theta}{\partial n} = 0 \tag{2.38}$$

2. The following is set for velocity profile and pressure:

$$\text{Inflow and outflow boundaries :} \qquad \frac{\partial u_1}{\partial y} = 0, \quad \frac{\partial u_2}{\partial y} = 0, \quad p = 0 \tag{2.39}$$

$$\text{Solid wall, } y = 0: \qquad u_1 = 0, \quad u_2 = 0, \quad \frac{\partial p}{\partial x} = 0 \tag{2.40}$$

$$\text{Top boundary, } y = 4: \qquad u_1 = 1, \quad \frac{\partial u_2}{\partial y} = 0, \quad p = 0. \tag{2.41}$$

Chapter 3

Results and discussion

3.1 Dendritic growth without convection in 2D

As a starting point we are interested in the two dimensional dendritic growth of the crystal without convection. Both isotropic and anisotropic cases are simulated. The computational domain is 2D box $(-4 \leq x \leq 4) \times (0 \leq y \leq 4)$. The equations (2.1) and (2.2) is simulated with the following initial parameters: the sharp interface parameters is taken as $\mu = 117.5$, anisotropy parameter was $\epsilon = 0.005$ and $d_0 = 0.001191$, the typical case of undercooling is assumed, $\theta_\infty = -0.5$.

As mentioned above, the Gibbs-Thomson kinetics at the interface is $-\theta_i = V/\mu + d_0/R$, where R is the local radius of curvature and V is the normal speed of the interface. In [6], it has been shown that by solving equations (2.24), (2.25) and using jump condition, (2.29), the following formula can be obtained:

$$-\theta_i = \frac{\tau V}{W\lambda} + \frac{1}{R}\frac{W}{\lambda}, \tag{3.1}$$

Using this relation and specification of a desired interface width, the phase field parameters λ, τ and W are determined: the interface thickness $W = 0.02$, capillary length $\lambda = 16.792$, kinetic undercooling $\tau = 0.002858$, also, $\Delta_c = 0.5$, $\kappa = 1$, $Err_{Fact} = 3$, $Err_{Fact_2} = 4$. The initial value is chosen as a circle with radius $r = 0.03573$ at the origin.

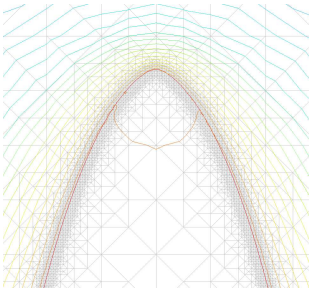

Figure 3.1: Isotherms around the tip

The discontinuity integrals occurring in the interface are computed as the formulation from previous chapter. Simulation is done for times from 0 to 0.75, the shape evolves into typical needle crystal, where the tip attains a nearly parabolic shape and a constant speed. The Figure 3.1 shows a close-up view of the tip region at the time $t = 0.75$. The temperature is quite smooth, and the jump in temperature is very well defined.

The temperature gradient changes over 1-2 elements at the interface and the region where the phase field varies is much wider then this.

The following figures describe the isotropic dendritic growth of the crystal in 2D, Figure 3.2.

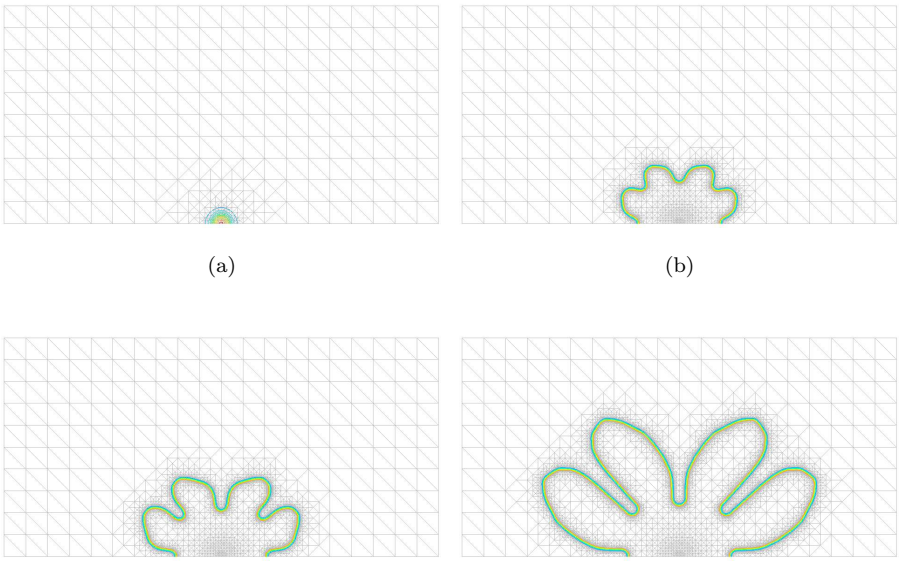

(a) (b)

(c) (d)

Figure 3.2: The phase field interface and mesh in different time: a) initial value, $t = 0$; b) $t = 0.5$; c) $t = 0.75$, d) $t = 1.6$

For anisotropic case, the modified 2D Laplacian (2.5) is included to the model and with the same parameters we obtain the results as the following figures, Figure 3.3.

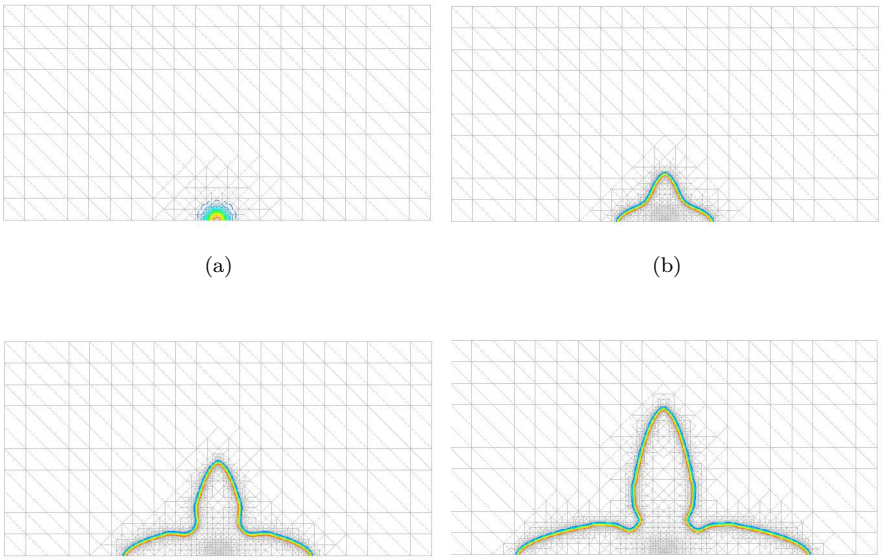

(a) (b)

(c) (d)

Figure 3.3: The phase field interface and mesh in different time: a) initial value, $t = 0$; b) $t = 0.25$; c) $t = 0.50$, d) $t = 0.75$

The simulation is done with different values of parameters. Our attention was focused in the shape of interface when different parameters are used. Obtained results showed that the shapes are almost the same and the entire history leading to this is the same, and does not depend on width parameter.

3.2 Convection effect to the 2D dendritic growth

Using the model constructed in chapter 1 we have done the simulations of the fluid flow around the dendrite with different values of Peclet and Prandtl numbers. Each simulation took a several hours in the computers AMD Athlon 1.667 MHz with Debian Linux in Department of Mechanics. For instance, the result described in figure 3.4 is computed almost is 24-28 hours. Also, speed of the program depends on selection of the smallest size of element in finite element refinements.

We say the upstream part of crystal positioned to the left of the tip of the vertical main stem, and another part of crystal is the downstream part.

The parameters used in our all simulations are: $\tau = 0.002858$, $\epsilon_p = 0.01$, $W = 0.02$, $\lambda = 16.792$, $\Delta_c = 0.5$, $\gamma = 0.05$, $Err_{fact} = 3$, $Err_{fact_2} = 4$.

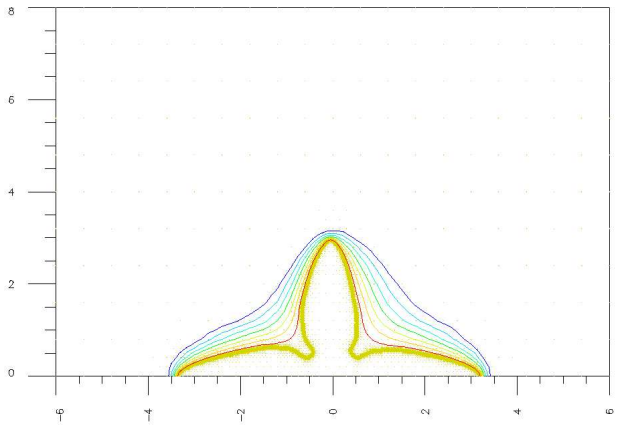

Figure 3.4: The solid/liquid interface at $t = 0.8$.. The parameters are: $\Delta_c = 0.5$, $Pe = 0.5$ and $Pr = 0.03$.

Figure 3.4 shows the solid/liquid interface and the isotherms for $Pr = 0.003$ and $Pe = 0.5$ at $t = 1$. The small asymmetry in the thermal field shows the convection affect. Since, Pectel number is small, the corresponding Reynolds number is also small. Therefore, the flow follows the interface without any effect to the main stem directions, but the sidebranches of the vertical main stem are promoted to grow on the upstream and downstream. When the $Pe = 0$ the sidebranches do not loose their symmetry, but with $Pe = 0.5$ the sidebranches have lost their symmetry even though the main stem evolves in the same way.

The following firgure 3.5 shows the case of $Pr = 0.03$ and $Pr = 3$ at time $t = 0.8$. Here it is obvious that the morphology of the crystal is quite different as the above figure. The corresponding Reynolds number is high enough to create a small separated vortex in the bulk. The vertical main stem starts to tilt towards the upstream direction. In the upstream, the direction of sidebranches of the main stem is rapid and also starts very close to the tip.

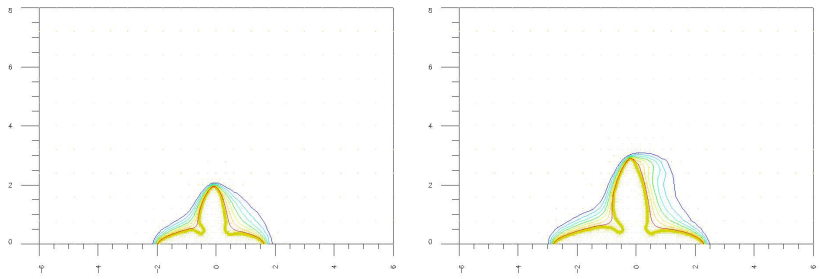

(a) (b)

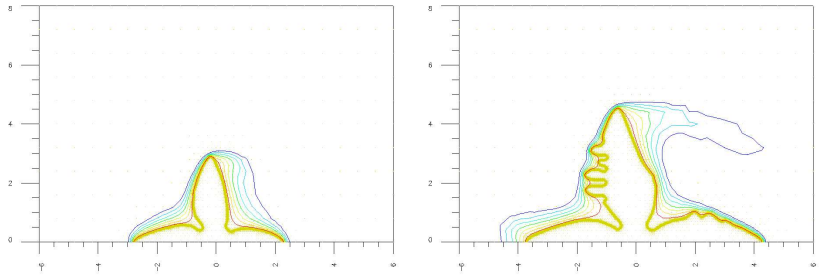

(c) (d)

Figure 3.5: The solid/liquid interface in different times: a) $t = 0.4$; b) $t = 0.6$; c) $t = 0.8$, d) $t = 1$. Innermost contour is solid/liquid interface and the other contours are isotherms for $\theta = -0.35, -0.3, -0.25, -0.2, -0.15, -0.1, -0.05$. The parameters are: $\Delta_c = 0.5$, $Pe = 3$ and $Pr = 0.03$.

The velocity is shown in the following figures, Firgure 3.6 and Firgure 3.7. It is easy to notice that there is a strong vortex behind the vertical tip. With higher Peclet number, the flow effects more the crystal. This can be seen in these two figures at the same time with different Pectel numbers:

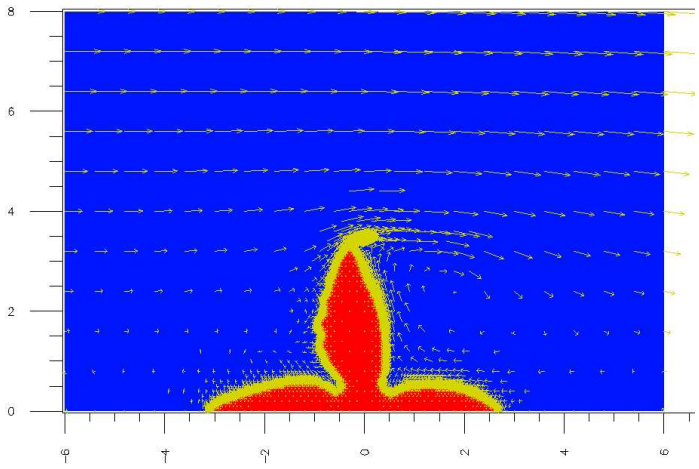

Figure 3.6: Velocity at $t = 0.7$ for $Pe = 3$

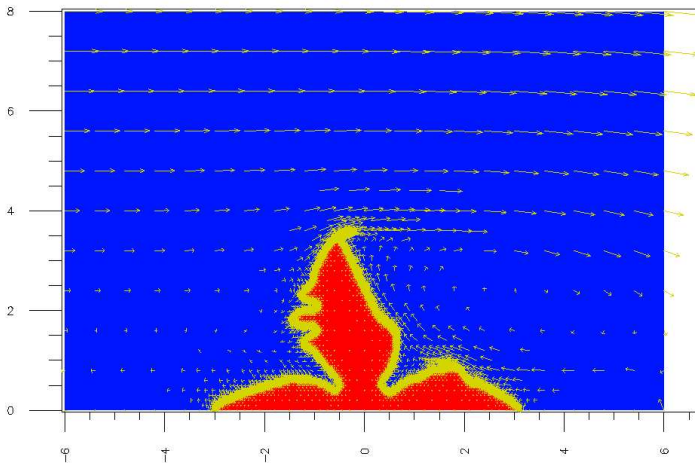

Figure 3.7: Velocity at $t = 0.7$ for $Pe = 5$

The simulations above show that for low Peclet number the growth is mainly controlled by the thermal diffusion. If the Peclet number increases, the sidebranches get controlled by the convection, the competitive growth and isothermal coarsening, and the vertical main stem start to tilt.

The simulation above is done with a low Prandtl number, because most of metals have $Pr < 0.1$. However many experiments are done with organic materials (SCN, PVA) and these have higher Prandtl number. Therefore, we are also interested in that and used higher Prandtl number in our simulation.

First, the program was run with $Pr = 23$ (SCN has the same Prandtl number) and $Pe = 2.5$. The small change occurs in morphology of the crystal and this is similar to the results of our first simulation, Figure 3.4.

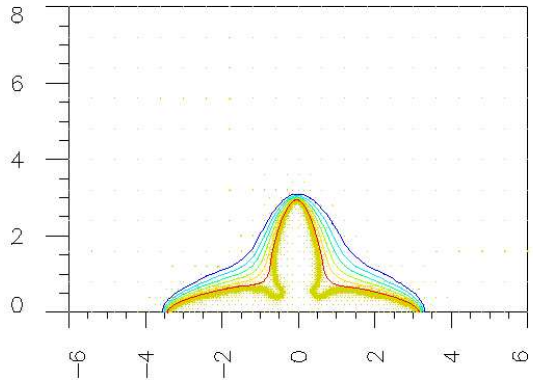

Figure 3.8: The solid/liquid interface at $t = 0.8$. The parameters are: $\Delta_c = 0.5$, $Pe = 2.5$ and $Pr = 23$.

Then, the Peclet number is increased to $Pe = 10$, Figure 3.9:

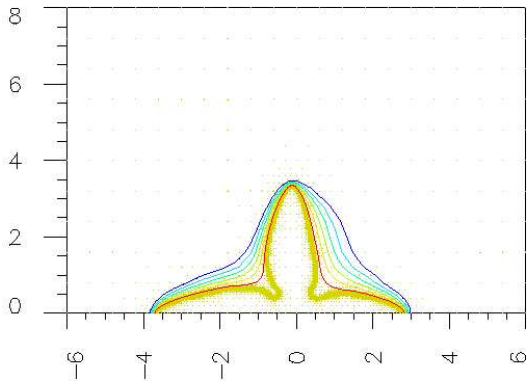

Figure 3.9: The solid/liquid interface at $t = 0.8$. The parameters are: $\Delta_c = 0.5$, $Pe = 10$ and $Pr = 23$.

The above simulations allow to conclude some important factors. The growth of the dendrite is controlled by heat transfer at the solid/liquid interface. When the forced flow is increased, the vertical main stem tilts increasingly towards the upstream direction. Also, the saidebranches on the vertical main stem are highly affected by the flow. The sidebranches at the upstream increase toward the flow, and the sidebranches on the downstream side are inhibited by the flow. At sufficient Pectel number the tip of the vertical main stem starts to split and this probably will finally resemble isotropic growth.

3.3 Three dimensional dendritic growth

The semisharp method in two dimensional case is simulated with and without convection. The results obtained in the above simulations are almost the same as results of standard phase field method. The same parameters as a [9] are used in the simulations, and the same influence of the convection is obtained.

Now, we are interested in three dimensional dendrite growth of the crystal. The three dimensional simulation without convection was studied by Irina Loginova [10], Karma [11], and with convection effect by Yili Lu, C. Beckermann and A. Karma [11], Jun-Ho Jeong, Nigel Goldenfeld and Jonatham A. Dantzig [12], using standard phase field model.

Irina Loginova [10] and A. Karma (and others) [11] studied the three dimensional dendritic growth by an adaptive finite difference method. The adaptive finite element method for standard phase field model is used in [12].

The interesting task is developing the semisharp phase field method into three dimensions. The discontinuity of temperature gradient at the interface is avoided by computing an integration over the surface. That helps us to know a solution of the model precisely at the interface. Thus, the interface thickness can be chosen a bit thicker.

As a test of written integration over the surface for discontinuity of gradient at the interface, we introduce the following Laplacian with a simple plane equation at three dimensional box $(-4 \leq x \leq 4) \times (-4 \leq y \leq 4) \times (0 \leq z \leq 4)$:

$$\begin{aligned} \nabla^2 u_1(x, y, z) &= 0, \\ u_2 &= x. \end{aligned} \tag{3.2}$$

The variation form for finite elements method including discontinuity integration is written as:

$$\int_\Omega \nabla v(x,y,z)\cdot\nabla u_1(x,y,z)d\Omega - \int_\Omega (DiscInt(u_2(x,y,z), 1\cdot v(x,y,z)))d\Omega = 0,$$
$$\int_\Omega v(x,y,z)u_2(x,y,z)d\Omega = \int_\Omega v(x,y,z)\cdot x d\Omega, \tag{3.3}$$

where $v(x,y,z)$ is the test function. The following figure obtained as a result, Figure 3.10.

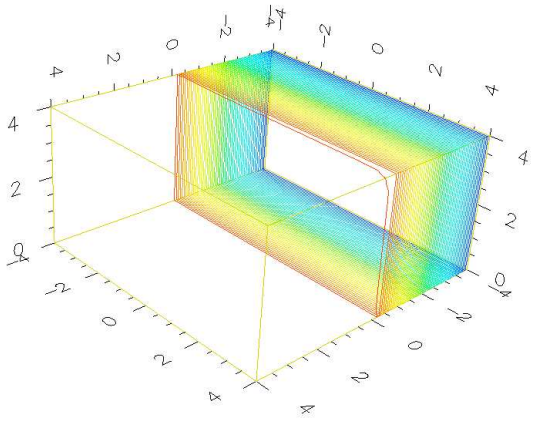

Figure 3.10: 3D solution to the equation (3.2)

The discontinuity integration is tested at the point $x = 0$. The result shows thatthe solution grows until this point, then stays constant.

The implementation of integration over the surface in Maple can be found from Appendix 3. The programming language C is used to derive the functions.

Then, the dendritic growth of the crystal is solved using semisharp phase field method is three dimensions. The tested above modification implemented into the model.

The sphere with radius $r = 0.03573$ is used as an initial value at the origin. An interface width and other parameters obtained from the relation (3.1) are chosen as the same value in two dimensions: $W = 0.02$, $\lambda = 16.792$, $\tau = 0.002858$. Other parameters used in adaptivity error control and anisotropy term are: $Err_{fact} = 3$, $Err_{fact_2} = 200$ and $\gamma = 0.05$. According to the stability, the time-step was $\Delta t = 0.000005$ initially, and it increases by one percent in each step until $\Delta t = 0.0005$. This speeds up the computations.

Both cases, isotropic and anisotropic dendritic growth are simulated. All calculations were made by computer Dexter in Department of Mechanics. Dexter is an AMD Opteron 144 1.8 GHz computer with 2 Gb memory that runs Debian Linux. The calculation of 3D isotropic dendritic growth took almost 50 hours. The computational domain is the box with size of$(0 \le x \le 2)\times(0 \le y \le 2)\times(0 \le z \le 2)$. The domain has initially 48000 elements (tetrahedrons) and 9261 nodes for isotropic case. These increase by adapting refinement on each time-step and at $t = 0.09$ mesh has 718246 elements and 128811 nodes.

The following figures are the results of isotropic dendritic growth using semisharp phase field method:

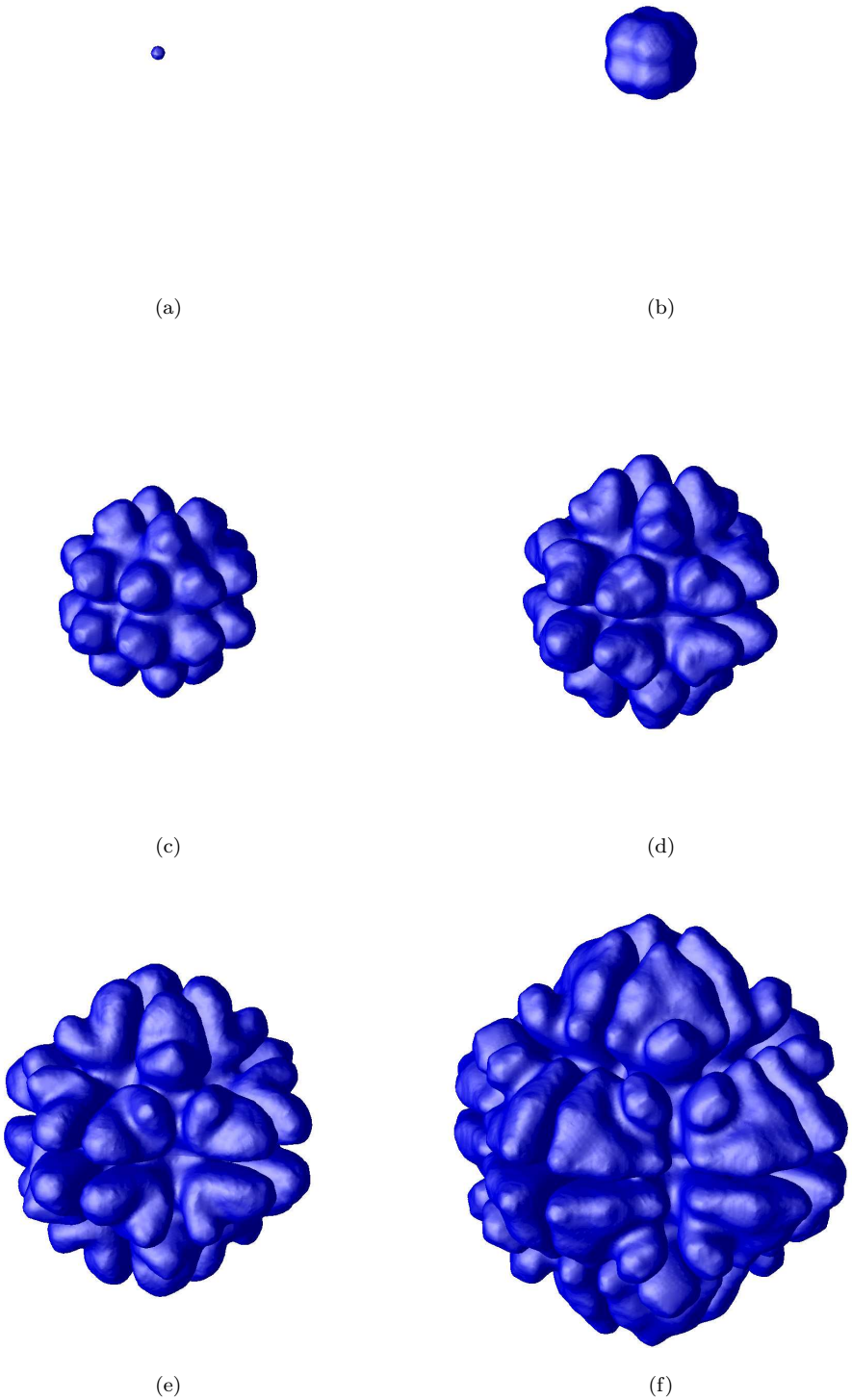

Figure 3.11: The solid/liquid interface on a $2 \times 2 \times 2$ cubic lattice in different times: a) $t = 0$; b) $t = 0.03$; c) $t = 0.045$, d) $t = 0.06$, e) $t = 0.075$, f) $t = 0.09$.

The simulation was performed in the first octant $(x, y, z \geq 0)$ with a spherical nucleus centered at the origin as an initial condition. The solid/liquid boundary shown here corresponds to the $\phi = 0$ surface reconstructed by the reflection about the $x = y = z = 0$ planes.

Then, the anisotropy dendritic growth is simulated. The initial condition is the same as isotropic case. Here, the 3D domain is refined into 162000 elements and 29791 nodes initially, and at time $t = 0.083$ it has 1115838 elements and 207416 nodes. The Figure 3.12 is the results of the simulation in different times. Compare with previous simulations, when using a standard phase field method, can say that the obtained results are almost the same.

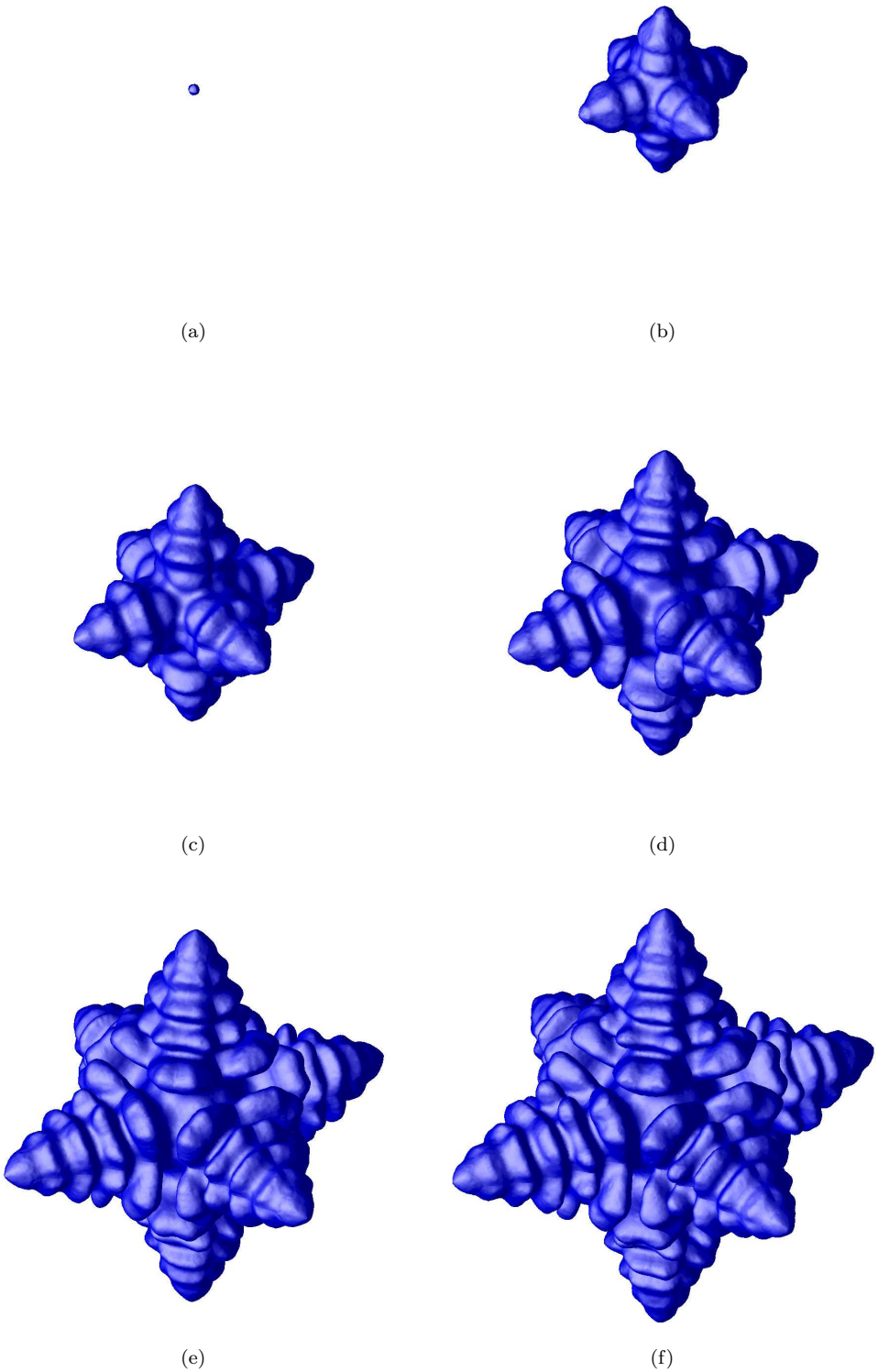

Figure 3.12: The solid/liquid interface on a $2 \times 2 \times 2$ cubic lattice in different times: a) $t = 0$; b) $t = 0.03$; c) $t = 0.045$, d) $t = 0.06$, e) $t = 0.075$, f) $t = 0.09$. The structure is seen from an angle where all six directions are visible.

Chapter 4

Conclusions

In this thesis the semisharp phase field method is studied for solving solidification problems in two and three dimensions.

First, the two dimensional dendritic growth of the crystal is studied without convection effects. The perfect results proved that the method can be used to study such problems. An important improvement is that the interface width is not so important for the solution of solid/liquid interface. This means, solution can be calculated exactly at the interface using techniques as of integration over the element in finite elements method. In standard phase field method, solution at the interface was calculated in the finite width - interface thickness. To have an accurate solution, the interface thickness should be chosen small, which is very expensive in calculation. Therefore, the modified method - semisharp much better for calculation and computation time, and it gives the same results as a standard phase field method.

Then, convection effect to the dendrite was in our focus. In order to observe, the convective effect simulations were done with different Peclet and Prandtl numbers. Obtained results showed, that with the increase of Peclet number the flow effects the dendrite increases too.

Generally, affected by flow, the vertical tip of a dendrite tilts increasingly towards the upstream direction, and the sidebranches on the vertical tip are also highly affected. The sidebranches on the left side of the vertical tip are promoted and the distance from the tip to the first sidebranches decreases as the Peclet number increases. However, the sidebranches on the right side of the vertical tip are inhibited by the flow and the distance from the tip to the first sidebranch increases as the Peclet number increases. Also, at sufficiently high Peclet number the tip of the vertical main stem starts to split and this probably, finally, will resemble isotropic growth. We observe that when the Prandtl number increases, the flow does not affect the dendrite.

Consequently, these results allow to conclude that, for $Pe > 1$ the flow controls the dendritic growth, otherwise, the heat diffusion controls the growth.

The more interesting task was simulation of three dimensional dendritic growth using the semisharp phase field method. Both isotropic and anisotropic cases were simulated, and one can say that the results are perfect and are the same as the results of standard phase field method. Anisotropy term in three dimensions was included in the model and gave the right solution.

All these results are obtained during the period allocated for the master thesis. We have other ideas too, however, the restricted time did not allow to pursue them here. For instance, since computation of the 3D code was too slow in a single computer, one can modify an existing parallel code to run in parallel computers. Then, convection effect could be included to the semisharp phase field method to study the differences, advantages, computational time and speed of the code with standard phase field method, which would be interesting.

As mentioned above repeatedly, the toolbox FemLego was used in all simulations. It helps to solve

several PDE's and avoid errors in inputting the formulations, easy to change the source code in C or FORTRAN according to certain problems. I would wish to see FemLego as a great software which helps to research and solve many scientific and realistic problems.

Bibliography

[1] C. Andersson. *Phase Field Simulation of Dentritic Solidification*. 2002: Doctoral Dissertatation. Department of Numerical Analysis and Computer Science, Royal Institute of Technology.

[2] Daniel M. Anderson and Geoffrey B. McFadden, ACMD. *A Phase-field Model for Contact Lines*. 1995: Summary of Activities, Applied and Computational Mathematics Division, Gaithersburg, USA. http://math.nist.gov/mcsd/Reports/95/yearly/

[3] B.T. Murray, A.A. Wheeler and M.E. Glicksman, J. *Crystal Growth*. 1995: p.386

[4] A.A. Wheeler. *Phase-field Theory of Edges in an Anisotropic Crystal*. 2006: Proceedings of the Royal Society. Published online (doi:10.1098/rspa.2006.1721).

[5] A. Karma, W.J. Rappel. *Quantitative phase-field modeling of dendritic growth in two and three dimensions*. 1998: The American Society, Physical Review E, volume 57, number 4. p.4323-4349.

[6] G.Amberg. *Semisharp Phase Field Method for Quantitative Phase Change Simulations*. 2003: The American Society, Physical Review Letters, volume 91, number 26.

[7] G.Amberg. *http://www2.mech.kth.se/ gustava/femLego*

[8] G.Amberg, Robert Tönhardt and Christian Winkler, *Finite Element Simulations using symbolic computing*. 1999: Mathematics and Computers in Simulation 49. p.247-274.

[9] Robert Tönhardt and Gustav Amberg, *Phase-Field Simulation of dendritic growth in a shear flow*. 1998: J. Crystal growth, 194, p.406-425.

[10] Robert Tönhardt and Gustav Amberg, *Simulation of natural convection effects on SCN crystals*. 2000: Physical Review E 62, p.828-836.

[11] Irina Loginova, *Phase-field modeling of diffusion controlled phase transformations*. 2003: Doctoral Thesis. Department of Mechanics, Royal Institute of Technology.

[12] Alain Karma and Wouter-Jan Rappel, *Numerical simulation of Three-Dimensional Dendritic Growth* 1996: Northeastern University, Boston.

[13] Yili Lu, C. Beckermann, A. Karma, *Convection effects in the three-dimensional dendritic growth* 2002: ASME International Mechanical Engineering Congress and Exposition, New Orleans, Louisiana.

[14] Jun-Ho Jeong, Nigel Goldenfeld and Jonatham A. Dantzig, *Phase-field model for three-dimensional dendritic growth with fluid flow* 2001: Physical review E, Volume 64, 041602.